chemosensors

Article

Influence of P(V3D3-co-TFE) Copolymer Coverage on Hydrogen Detection Performance of a TiO_2 Sensor at Different Relative Humidity for Industrial and Biomedical Applications

Mihai Brinza [1,2], Lynn Schwäke [1], Lukas Zimoch [3], Thomas Strunskus [1,4,*], Thierry Pauporté [5], Bruno Viana [5], Tayebeh Ameri [4,6], Rainer Adelung [3,4], Franz Faupel [1,4,*], Stefan Schröder [1,4,6,*] and Oleg Lupan [1,2,3,5]

1 Multicomponent Materials, Department of Materials Science, Kiel University, Kaiserstraße 2, D-24143 Kiel, Germany; mihai.brinza@mib.utm.md (M.B.); lysc@tf.uni-kiel.de (L.S.); oleg.lupan@mib.utm.md (O.L.)
2 Center for Nanotechnology and Nanosensors, Department of Microelectronics and Biomedical Engineering, Technical University of Moldova, 168 Stefan cel Mare Av., MD-2004 Chisinau, Moldova
3 Functional Nanomaterials, Department of Materials Science, Kiel University, Kaiserstr. 2, D-24143 Kiel, Germany; luzi@tf.uni-kiel.de (L.Z.); ra@tf.uni-kiel.de (R.A.)
4 Kiel Nano, Surface and Interface Science (KiNSIS), Kiel University, Christian Albrechts-Platz 4, D-24118 Kiel, Germany; tam@tf.uni-kiel.de
5 Institut de Recherche de Chimie Paris-IRCP, Chimie ParisTech, Université PSL, rue Pierre et Marie Curie 11, 75231 Paris Cedex 05, France; thierry.pauporte@chimieparistech.psl.eu (T.P.); bruno.viana@chimieparistech.psl.eu (B.V.)
6 Composite Materials, Department of Materials Science, Kiel University, Kaiserstraße 2, D-24143 Kiel, Germany
* Correspondence: ts@tf.uni-kiel.de (T.S.); ff@tf.uni-kiel.de (F.F.); ssch@tf.uni-kiel.de (S.S.)

Abstract: The detection of hydrogen gas is crucial for both industrial fields, as a green energy carrier, and biomedical applications, where it is a biomarker for diagnosis. TiO_2 nanomaterials are stable and sensitive to hydrogen gas, but their gas response can be negatively affected by external factors such as humidity. Therefore, a strategy is required to mitigate these influences. The utilization of organic–inorganic hybrid gas sensors, specifically metal oxide gas sensors coated with ultra-thin copolymer films, is a relatively novel approach in this field. In this study, we examined the performance and long-term stability of novel TiO_2-based sensors that were coated with poly(trivinyltrimethylcyclotrisiloxane-co-tetrafluoroethylene) (P(V3D3-co-TFE)) co-polymers. The P(V3D3-co-TFE)/TiO_2 hybrid sensors exhibit high reliability even for more than 427 days. They exhibit excellent hydrogen selectivity, particularly in environments with high humidity. An optimum operating temperature of 300 °C to 350 °C was determined. The highest recorded response to H_2 was approximately 153% during the initial set of measurements at a relative humidity of 10%. The developed organic–inorganic hybrid structures open wide opportunities for gas sensor tuning and customization, paving the way for innovative applications in industry and biomedical fields, such as exhaled breath analysis, etc.

Keywords: sensors; organic–inorganic structures; hybrid gas sensor; tuning; hydrogen; copolymer; PTFE; PV3D3; P(V3D3-co-TFE)

check for updates

Received: 24 February 2025
Revised: 10 April 2025
Accepted: 15 April 2025
Published: 19 April 2025

Citation: Brinza, M.; Schwäke, L.; Zimoch, L.; Strunskus, T.; Pauporté, T.; Viana, B.; Ameri, T.; Adelung, R.; Faupel, F.; Schröder, S.; et al. Influence of P(V3D3-co-TFE) Copolymer Coverage on Hydrogen Detection Performance of a TiO_2 Sensor at Different Relative Humidity for Industrial and Biomedical Applications. *Chemosensors* **2025**, *13*, 150. https://doi.org/10.3390/chemosensors13040150

Copyright: © 2025 by the authors. Licensee MDPI, Basel, Switzerland. This article is an open access article distributed under the terms and conditions of the Creative Commons Attribution (CC BY) license (https://creativecommons.org/licenses/by/4.0/).

1. Introduction

Gas sensors are of great interest in many applications. They enable monitoring and control in industrial applications, but also in areas such as medicine, food, automotives, agriculture, or domestic use [1–3]. In recent years, hydrogen monitoring has become very important. Hydrogen is a clean and versatile energy carrier [4], enabling affordable

and sustainable modern energy [5,6]. As reported in the literature, there are a multitude of methods of hydrogen production [4] and storage [7], which typically involve high pressure and/or low temperature. These factors, in combination with inadequate long-term monitoring and non-rapid leak detection, pose a significant danger to humans and nature alike, limiting the safe usage of hydrogen for industrial applications. Beyond its industrial applications, hydrogen has been used in the pharmaceutical industry [5] for the manufacture of specific drugs [8] and for producing hydrogen peroxide, which is a key chemical and oxidant [9]. Furthermore, hydrogen use is surging as a therapeutic gas, e.g., as a treatment for reperfusion or re-oxygenation injury [10]. Hydrogen therapy is additionally recognized as a treatment for neurodegenerative diseases, rheumatoid arthritis, diabetes mellitus, brain stem infarction, cancer, as well as exercise- or sports-induced oxidative stress [11,12]. Several different modes of administration are known for these treatments [13,14], some of which lead to detectable changes in exhaled air [15]. In addition, hydrogen is a potential biomarker for irritable bowel syndrome starting from 12 ppm [16,17] and lactose intolerance if there is an increase of 20 ppm above the baseline [15,18,19], which extends the use of hydrogen gas sensors to the field of diagnostics. Thus, hydrogen is used in a wide variety of fields, especially in industry and in the medical field.

However, for monitoring and control in these application areas, long-term, stable, fast responding, and highly sensitive hydrogen gas sensors are required. In addition, the sensors should be essentially unaffected by external factors such as the presence of other gases or humidity. The latter property in particular poses a challenge for state-of-the-art sensor materials such as TiO_2, resulting in the introduction of polymer-coated hybrid sensors [15,20–25].

In this study, TiO_2 was selected as a sensor material due to its recognized stability over extended time periods [26–29], which has led to its utilization in hydrogen gas sensors that exhibit a time-independent gas response [26,30–32].

However, further investigation is essential to increase the stability and reduce the interference of relative humidity (RH) to improve reliable long-term operation, since RH significantly affects sensor performances and capabilities. For example, it is important to note that relative humidity is the main cause of the lack in performance of metal oxide sensors [33–35].

Although TiO_2 is sensitive to hydrogen [36], its gas sensing performance can be negatively affected by external factors too, like humidity, etc. [26]. The effects of humidity on the magnetic properties and electrical conductivity of semiconductors are well known and have been a major challenge for the last decades [37,38]. Hybrid structures open new opportunities for gas sensor tuning and customization, as well as immunization vs. humidity [39], paving the way for innovative applications in industry and biomedical fields, such as exhaled breath analysis.

Combining different nanomaterials with excellent mechanical and electronic properties creates composite materials of great technological interest, as adding a second phase can significantly enhance their capabilities, including electronic [40] and sensing performance, especially in humid ambients [33,40] and by mixing with ternary phases [41].

Researchers use different approaches to obtain practical promising compounds as electronic materials such as different mixes of metals and oxides [42]. While this research path takes into account the addition of a second phase [40] and considers the deviation of the original cations of the metals used [43] or even puts an emphasis on the effect of crystallite size and distribution [44], it is also possible to obtain promising composite materials by using different polymer and copolymer coatings [15,20,21,45,46].

The coating of semiconducting metal oxide gas sensing structures with polytetrafluoroethylene (PTFE) and poly(trivinyltrimethylcyclotrisiloxane) (PV_3D_3) thin films leading

to organic–inorganic hybrid gas sensors appears to be of great interest for hydrogen detection. The former is a fluorine-based polymer that exhibits high hydrophobicity, which can have a positive effect on the long-term stability of sensor performance, especially in humid environments like in exhaled air, etc. In addition, PTFE coatings have shown an effect on sensor selectivity [46]. However, their operation temperature is limited due to the fact that PTFE shows phase transitions in its semicrystalline regions and its onset of degradation starts gradually at around 260 °C, followed by rapid degradation at 400 °C and higher [47–49]. Hybrid gas sensors with PV_3D_3 retain their hydrophobicity even after annealing at 400 °C [39]. While individual PTFE/TiO_2 and PV_3D_3/TiO_2 hybrid gas sensors have been investigated previously by us, a copolymer coating combining the promising properties of both polymers has not been analyzed for gas sensor applications. Furthermore, no information on their long-term stability with regard to gas sensing has been reported so far.

Consequently, this gap is addressed in the current work. Aiming for enhanced long-term stability, overall performance, and specifically tailored sensitivity [20,39,45] in a humid environment, we fabricated a sensor based on a TiO_2 nano-layer entirely coated with an ultra-thin P(V_3D_3-co-TFE) copolymer film via solvent-free initiated chemical vapor deposition (iCVD) [50], referred to as a P(V_3D_3-co-TFE)/TiO_2 hybrid gas sensor. Its gas sensing performance was studied and monitored over a total time span of 427 days to investigate its long-term performance. The hydrophobic nature of the hybrid sensors prevents the recorded data from being influenced by moisture and the environment, providing the next step towards the detection of hydrogen as a biomarker in exhaled air.

2. Materials and Methods

2.1. Sample Production

The hybrid gas sensor principle in this study is similar to the one described in our previous works [20,45]. A quartz or glass substrate (Thermo scientific, 2.6 × 7.6 cm, Menzel-Gläser, Braunschweig, Germany) was precleaned by dipping it into a HCl solution (10%), followed by rinsing it with deionized water in an ultrasonic bath. It was then placed on a heating plate at 445 °C for 15 min. TiO_2 was deposited on this substrate by spray pyrolysis as described by Pauporté et al. [51]. Subsequently, the samples were thermally treated at 450 °C for another 30 min and cooled down naturally. The resulting 20 nm thick TiO_2 sprayed layer was post treated thermally for 60 min at 610 °C in air to decompose all residue materials from the surface and stabilize the crystalline phase [52]. Lastly, Au-interdigital electrodes were sputtered on top through a meander shaped shadow mask with a gap of 1.0 mm [53]. To avoid confusion, all production details for the sensor are indicated directly in the figure captions as well as in the related discussion parts.

The gas sensors, consisting of a TiO_2 nanolayer with Au contacts, were subsequently coated with a copolymer thin film to protect them from the environment, moisture, and humidity, and to tailor their gas sensing selectivity and performances. The deposition of 25 nm thick P(V_3D_3-co-TFE) copolymer thin films was performed using a custom-built iCVD reactor. The technical details are described elsewhere [39]. V_3D_3 and HFPO monomers were combined with the initiator perfluorobutanesulfonyl fluoride (PFBSF) to produce the polymer thin films. This combination has already been demonstrated in the literature [54]. The flow rates for V_3D_3, HFPO, and PFSBF during the deposition process were 0.2 sccm, 0.2 sccm, and 0.1 sccm, respectively. The substrate temperature was 30 °C and the process pressure 40 Pa. The filament array inside the reactor was resistively heated by applying 3.1 A and 16.7 V to the filament. The deposition rate was 1.8 nm/min. We refer to as P(V_3D_3-co-TFE)/TiO_2/quartz hybrid gas sensors for the fabricated organic–inorganic structures in the following text.

After fabrication and between measurements, the samples were stored in opaque containers that had been lined with paraffine paper under ambient conditions. The heating of the sensors before usage after long-term storage can be beneficial for several reasons. During storage, the sensor surface (especially metal oxides or porous materials) can adsorb moisture, hydrocarbons, or other environmental contaminants. Long storage periods may cause the sensor's baseline signal to drift. Thermal treatment at 300 °C can help to stabilize the baseline before measurements begin, reducing initial response fluctuations.

2.2. Computational

A section of the molecular structure of the P(V_3D_3-co-TFE) copolymer structure was modelled in Avogadro version 1.99.0. Geometry optimization of the obtained structure was performed via universal force field (UFF) [55]. Molden version 6.4 was used to visualize the output.

2.3. Sample Characterization

The sensing performances to test gas were performed using a heterostructured detector connected to interdigital gold electrodes, as can be observed in Figure 1, where (a) represents a schematic of the studied sensor. Figure 1b shows a magnified image of the meander architecture and (c) the proposed schematic sensing structure. The measuring apparatus was linked to a set-up with gas flow as described in our previous works [56–59].

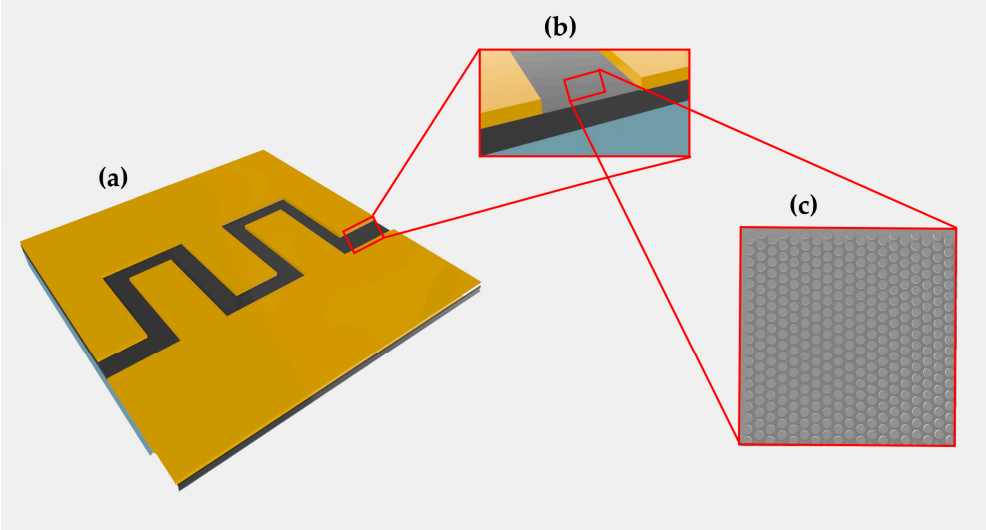


Figure 1. Schematic representation of the developed hybrid sensor with a gap of 1 mm between gold electrodes: (**a**) top view of the studied sample showing Au contacts/electrodes with meander shape on hybrid surface of sensor nanomaterial; (**b**) a magnified image of the meander architecture in cross-sectional view of the gas sensor and (**c**) top view of the proposed schematic sensing structure, namely of polymer/oxide coated gas sensing structure.

The gas response S for each dataset was calculated according to Equation (1), which was also mentioned in previous research [45], where a percentage-based ratio was obtained from electrical conductance, namely G_{gas} and G_{air}. This equation is based on the conductance G and calculated from Equation (2). R_{air} represents the resistance of the sample in air for G_{air} and in the same way R_{gas} for G_{gas} (influenced by applied gas).

$$S = \frac{G_{gas} - G_{air}}{G_{air}} 100\% \quad (1)$$

$$G_{air} = \frac{1}{R_{air}} \quad (2)$$

The gas response of the sample was measured using a custom setup and protocol based on a computer-controlled Keithley 2400 source-meter described in our previous works [20,26,33]. While varying the operating temperature (OPT), volatile organic compounds (VOCs) and hydrogen were used as test gases or vapors with a flow of 500 sccm (mL/min) of ambient gas (synthetic air) to obtain optimum sensor response. Furthermore, the described setup was utilized to assess dynamic responses, while maintaining a constant operation temperature. This enabled the determination of reaction times τ_r and recovery times τ_d, extracted from the first applied vapor pulse. Considering the lack of regulation, a feeding gas flow was supplied from a cylinder with a specific concentration and then adjusted using pre-calibrated mass flow controllers [58–60]. The required concentrations were obtained using Equations (3) and (4) to evaluate the sensor performances for the specimen [61–64]:

$$C\ (ppm) = \frac{C_1 \cdot F_{gas}}{F_{tot}} \quad (3)$$

where C is the required concentration of gas, C_1 is the initial concentration of the test gas, and F_{gas} is the gas flow. F_{tot} is the total flow of the gas–air mixture [33].

$$V_x = (Vol \cdot C \cdot M)/(22.4 \cdot d \cdot p) \cdot [(273 + T_r)/(273 + T_c)] \cdot 10^{-9} \quad (4)$$

where V_x is the volume of VOC injected into the test chamber volume Vol. C is the required VOC concentration (ppm), M is the molar mass, d is the density (g/cm^3), p is the purity, T_r is the room temperature, and T_c is the test chamber temperature (operating temperature).

In addition, the limit of detection (LoD) of the sensors for different temperatures and relative humidity was determined using Equation (5) [65]:

$$LoD = 3\frac{\sigma_B}{b} \quad (5)$$

The symbol σ_B is the population standard deviation of the blank signals, b is the slope of the signal/concentration functional relationship, and '3' is the chosen expansion factor. Origin software's linear fit function, in OriginLab 2024, was used to determine both the standard deviation and the slope.

Different levels of relative humidity (RH) were generated using a bubble humidification setup. This process entailed the passage of air through deionized water, followed by its continuous injection into the measurement chamber to generate the necessary RH value. The humidity was continuously monitored by a standard hygrometer. More details can be found in previous works [26,33,58,66]. In addition, relative humidity was measured continuously throughout the experiment using a specialized, calibrated sensor (SHT43; Digital Humidity Sensor with ISO17025 certification) placed next to the sample [33,58,66,67].

Fourier-transform infrared (FTIR) spectra of two P(V_3D_3-co-TFE) co-polymer thin films deposited onto Si substrates were measured using a FTIR spectrometer (Bruker Invenio R, Billerica, MA, USA). The first sample set was an as-deposited 260 nm thick film for reference, while the second sample set was heated to 350 °C for 15 min, simulating the sensor's measurement conditions. The spectra were recorded from 7500 to 368 cm^{-1} with 32 scans at 4 cm^{-1} resolution. A range from 4000 to 500 cm^{-1} was selected for further investigation. Baseline correction (spline), atmospheric compensation (CO_2), normalization, and smoothing (Savitzky–Golay) were performed on the recorded data using the Origin software (OriginLab 2024).

3. Results and Discussion

The fabricated P(V_3D_3-co-TFE) hybrid sensors were investigated with regard to their chemical and the gas sensing properties. All applied gases had a concentration of 100 ppm.

3.1. Chemical Characterization of the Fabricated Hybrid Sensors

During the iCVD process, V_3D_3 adsorbs at the substrate stage and HFPO and the initiator PFBSF are thermally decomposed to yield, e.g., difluorocarbene and fluorobutane radicals, respectively. Consequently, the difluorocarbene as well as the initiator radicals can initiate the polymerization via the vinyl groups of V_3D_3. Thus, using V_3D_3 and HFPO as co-monomers, we expected a molecular structure in which the CF_2 chains are connected by V_3D_3 crosslinks between the chains, resulting in sieve-like structures as schematically illustrated in Figure 2a.

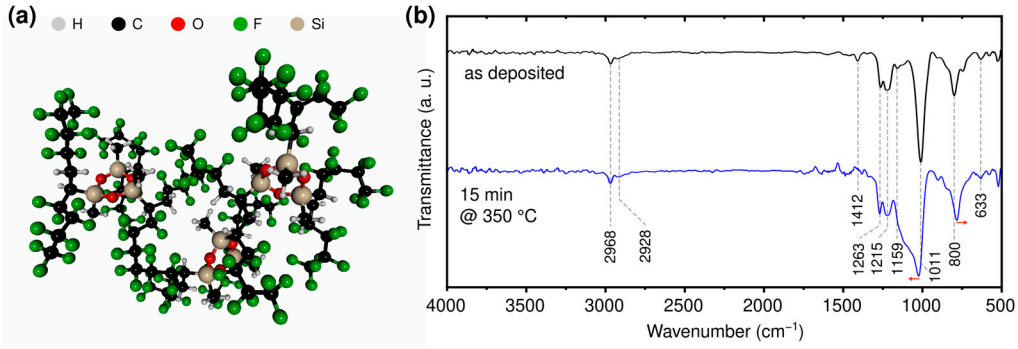


Figure 2. (**a**) Visualization of the molecular structure inside the deposited P(V_3D_3-co-TFE) thin films. (**b**) FTIR spectra of an as-deposited P(V_3D_3-co-TFE) thin film (black curve) and a P(V_3D_3-co-TFE) annealed at 350 °C in air for 15 min (blue curve). Red arrows indicate a change in position of the cyclotrisiloxane ring-associated band in the FTIR measurement.

iCVD as a solvent-free process allows the combination of co-monomers, which lack a common solvent needed in wet-chemical preparations. To confirm the functionality of both co-monomers inside our polymer films, we performed FTIR measurements shown in Figure 2b. The as-deposited 260 nm P(V_3D_3-co-TFE) (black curve) copolymer layer revealed C-H stretching bands between 3000 cm^{-1} and 2800 cm^{-1} for the formation of sp^3 hybridized carbon links and thus the successful incorporation of V_3D_3 units inside the polymer film. The cyclotrisiloxane rings of V_3D_3 were preserved during the polymerization, indicated by the band at 1011 cm^{-1} for the as-deposited film. Additional bands corresponding to Si-CH_3 symmetric as well as asymmetric bending and rocking vibrations can be observed at 1263, 1412 and 800 cm^{-1}, respectively [54]. The 1412 cm^{-1} band can also be associated with Si-CH_2 groups [68], which indicates the expected crosslinking via reacted vinyl groups.

Fluoropolymer functionalities are shown by the bands at 1215, 1159, and 633 cm^{-1} [54,69]. This reveals a successful formation of a P(V_3D_3-co-TFE) polymer film. The 1:1 ratio of V_3D_3 and HFPO flows should ideally result in an equal number of V_3D_3 and the TFE units in the copolymer. However, the strong bands related to V_3D_3 indicate a higher density of V_3D_3 units inside the film.

In order to simulate the conditions that are present during the gas sensing measurement, the sample was heated to 350 °C for a period of 15 min in ambient air. The purpose of this experiment was to investigate whether a chemical modification of the film occurs during the gas sensing measurement. After heat treatment at 350 °C, the deposited film is reduced in thickness, resulting in a reduced signal-to-noise ratio. Furthermore, a change in position of the cyclotrisiloxane ring-associated band can be noted in the FTIR measurement (blue curve in Figure 2b). A shoulder is formed, while the band shifts towards larger wavenumbers, indicated by the small red arrow in Figure 2b. Additionally, the Si-CH_3

rocking associated band shifts towards smaller wavenumbers. These phenomena can be attributed to structural changes within the thin film, such as an increase in Si-O-Si bond angle, indicating a change from a ring towards a cage structure of the crosslinking unit [70] or opening of the ring structure, which is beneficial for sensor applications. The PTFE-associated bands do not appear to undergo substantial alterations, suggesting that there is no significant decomposition of this component.

3.2. Gas Sensing Measurements and Evaluation

The first set of gas sensing measurement results of the P(V_3D_3-co-TFE)/TiO_2 hybrid gas sensor is shown in Figure 3, which shows an entire set (a) at 10% RH and the dynamic responses at the best response operating temperatures (b,c). The measurement conditions were set to 10% RH due to the potential relevance of gas detection in low RH environments to various application fields, particularly in biomedicine and food storage [71–74]. For instance, cleanrooms are frequently operated within the range of 10–20% RH to mitigate the risk of electrostatic discharge (ESD) [75,76] and/or to enhance virus attenuation [77,78]. Figure 3a shows the measured sensor response of our hybrid structure at different operating temperatures at 10% RH. This sensor structure shows the best results for hydrogen gas with a response value of ~153% at an operating temperature of 300 °C.

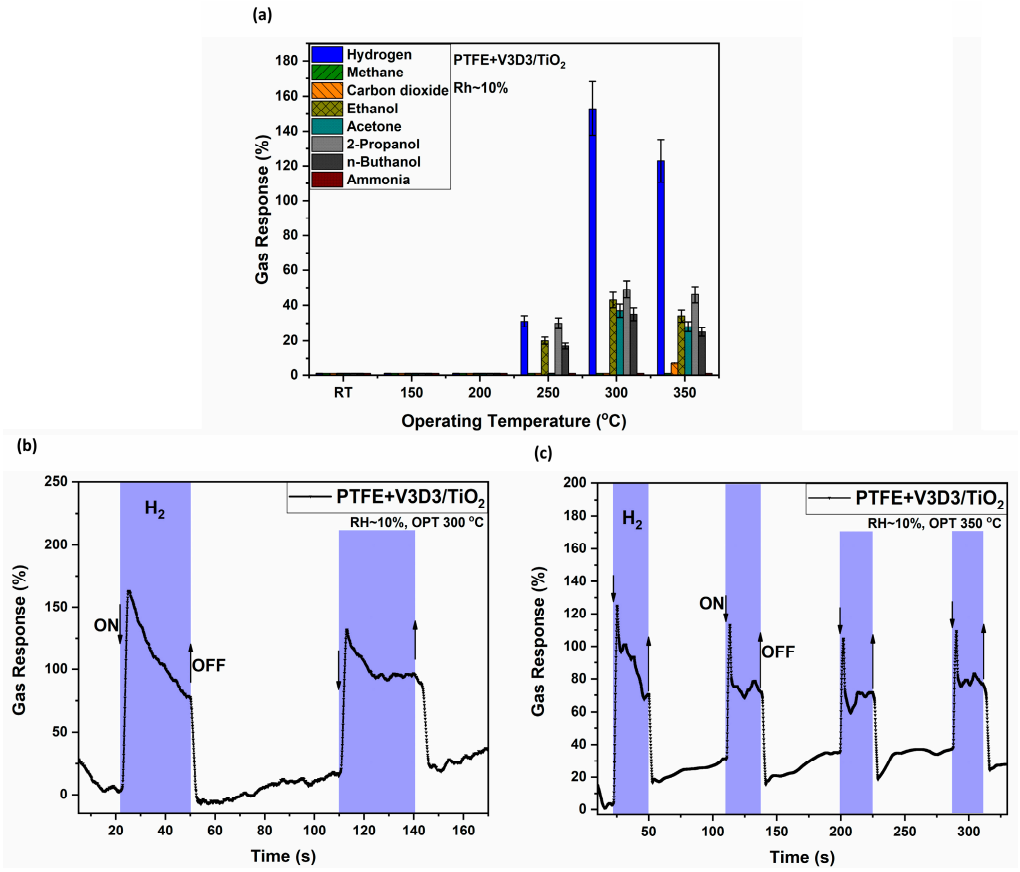


Figure 3. (**a**) Experimental measurements of the gas response of the P(V_3D_3-co-TFE)/TiO_2 hybrid structure to different gases and VOCs (hydrogen, methane, carbon dioxide, ethanol, acetone, acetone, 2-propanol, n-butanol, ammonia) at different operating temperatures. (**b**) Dynamic response of the same structure to hydrogen gas (100 ppm concentration) at 10% RH and operating temperatures of 300 °C and (**c**) 350 °C.

A similar selectivity is maintained at operating temperatures of 250 °C and 350 °C with reduced gas responses of ~30 and ~123%, respectively. At elevated temperatures, ethanol, n-butanol, 2-propanol, and acetone vapor were detected, with relatively low gas

response values. Consequently, an operating temperature of 300 °C was selected for the analysis of the dynamic respons to hydrogen (Figure 3b). Our hybrid sensor exhibits a ~153% response in combination with a relatively promising reaction time of τ_r = 2.0 s and recovery time of τ_d = 2.1 s. For comparison, Figure 3c depicts the dynamic response at an elevated operating temperature of 350 °C. At this temperature, a slightly reduced gas response of ~123% is observed, yet faster reaction and recovery times of τ_r = 0.5 s and τ_d = 1.6 s are noted.

To investigate the long-term stability, we reevaluated the same sample 309 days after the first measurements for the same gases. We chose the same environment (10% RH) as well as an environment with higher relative humidity (45% RH) (Figure 4) in a similar way as in previous studies [33,58]. Before measurement, the hybrid sensors were heated/thermally treated to remove moisture, hydrocarbons, or other environmental contaminants from their surfaces, as described in Section 2.1. The hybrid sensors are fabricated to work in real-world environments. Thus, it is not necessary to store them in inert gas or a vacuum.

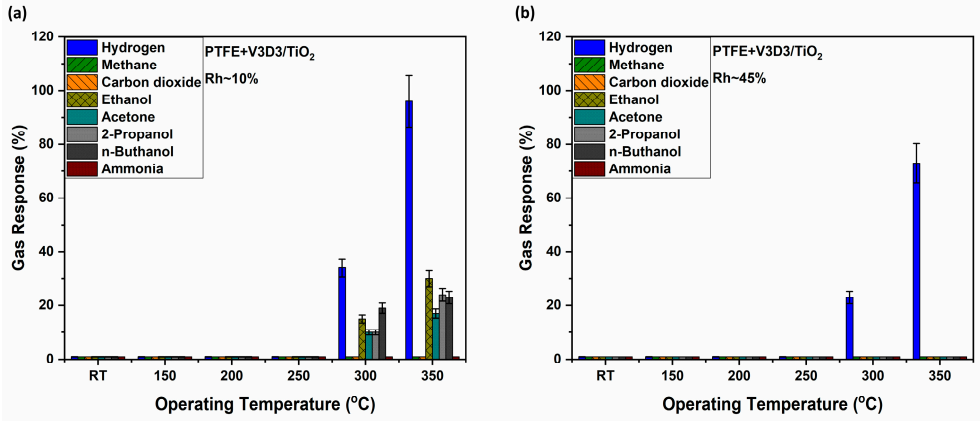


Figure 4. The gas response of the P(V_3D_3-co-TFE)/TiO_2 hybrid structure after 309 days from first measurements for different gases and VOCs (hydrogen, methane, carbon dioxide, ethanol, acetone, acetone, 2-propanol, n-butanol, ammonia) at different operating temperatures. (**a**) shows the results obtained in a relative low humidity of ~10% RH and (**b**) shows those obtained at ~45% ambient relative humidity.

Figure 4a shows that even after 309 days, a clear detection of ethanol, n-butanol, 2-propanol, acetone, and especially hydrogen gas is observed at elevated temperatures. Thereby, in comparison to Figure 3a, the optimal gas response for hydrogen gas shifted towards higher operating temperatures, with slightly reduced response values of 34% and 96% at 300 °C and 350 °C, respectively. A rise in relative humidity keeping all other measurement conditions constant results in a general decrease in gas response (Figure 4b), which could occur due to a specific gas sensing mechanism at higher operating temperature [34,79], which has to be investigated in more detail in the future. A hydrogen gas response of ~23% at 300 °C and ~73% at 350 °C is observed, indicating a decrease of about ~11% and ~23%, respectively, due to relative humidity increase. The gas response decrease for other test gases and VOCs is significantly higher, resulting in an improved hydrogen gas selectivity of the presented hybrid sensors in high humidity environments.

Again, an operating temperature of 300 °C as well as 350 °C was selected for the analysis of the dynamic response to hydrogen at 10% and 45% RH (Figure 5). A 34% hydrogen gas response at 10% RH and 300 °C was measured. In addition, reaction and recovery times of τ_r = 3.0 and τ_d = 4.9 s were determined (Figure 5a). An increase of relative humidity to ~45% RH, again, leads to a decreased hydrogen gas response value of ~23% and response and recovery times of τ_r = 4.2 s and τ_d = 4.4 s, respectively (Figure 5b). Furthermore, it can be noted that the signal became slightly unstable, which is assumed

to be due to the abundance of water molecules on the top surface of the sensor structure. Figure 5c shows the dynamic response data for 10% RH and 350 °C operating temperature. The higher operation temperature had a positive influence on the hydrogen gas response value (approximately 96%). The response and recovery times are τ_r = 1.3 s and τ_d = 2.1 s, respectively. An increase in humidity (45% RH) leads again to a reduced hydrogen response value (approximately 73%) and response and recovery times of τ_r = 2.3 s and τ_d = 3.3 s (Figure 5d).

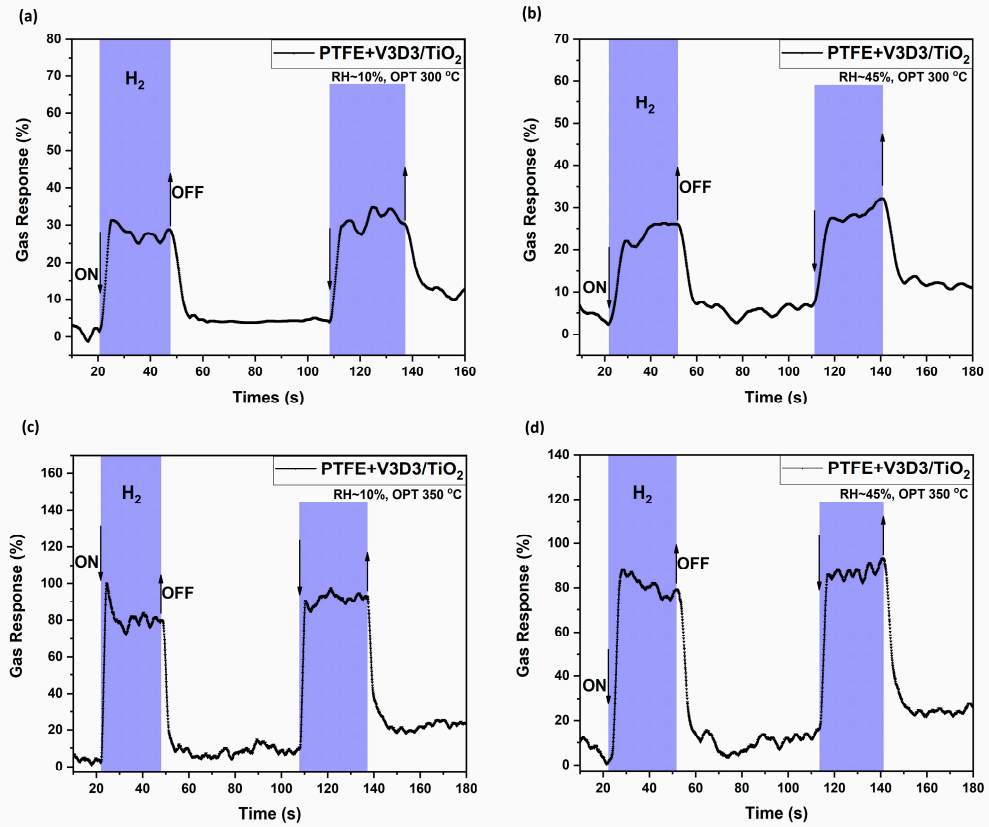


Figure 5. Dynamic response to hydrogen gas of a P(V_3D_3-co-TFE)/TiO_2 hybrid structure investigated 309 days after its first measurements. The individual subplots show the measurements at different operating temperatures and different relative humidity values: (**a**) 300 °C, ~10% RH; (**b**) 300 °C, ~45% RH; (**c**) 350 °C, ~10% RH, and (**d**) 350 °C, ~45% RH.

Unlike the overall gas responses, the reaction and recovery times seem to exhibit no significant changes with humidity or temperature. At higher relative humidity levels, the recorded signal shows slight perturbations manifested as different "noise hills" between the pulses. Nevertheless, the overall signal maintains a consistent shape. As noted in a recent review [80], low-frequency noise can stem from various sources and be impacted by numerous parameters, including, e.g., the sputtering power used during the fabrication process [81], etc. In our situation, the noise could originate from the fabrication process as well, specifically from the interface formed between the copolymer film and the gas sensing structure. This interface could cause vapor molecules to move chaotically, occasionally resulting in low-frequency noise. Due to the intricate nature of the noise phenomenon and the numerous potential causes, a definitive conclusion cannot be provided at this stage. Further research is necessary to understand the underlying mechanisms and identify the specific factors contributing to the noise phenomenon.

After an additional 118 days after the second measurement (after 427 days in total), we tested the hybrid structure again using the same gases, VOCs, and environments (10% RH and 45% RH). The corresponding gas responses and dynamic hydrogen responses at

300 °C and 350 °C are shown in Figures S1 and S2. These data support the trend observed during the second measurement (Figure 5), highlighting the high hydrogen gas selectivity in high humidity environments. As time progresses, the overall hydrogen gas response of the analyzed hybrid sensor exhibits a decline, as shown in (Figure 6). After a period of 427 days, the hydrogen gas response is reduced to approximately 28% at 300 °C and 75% at 350 °C operating temperature.

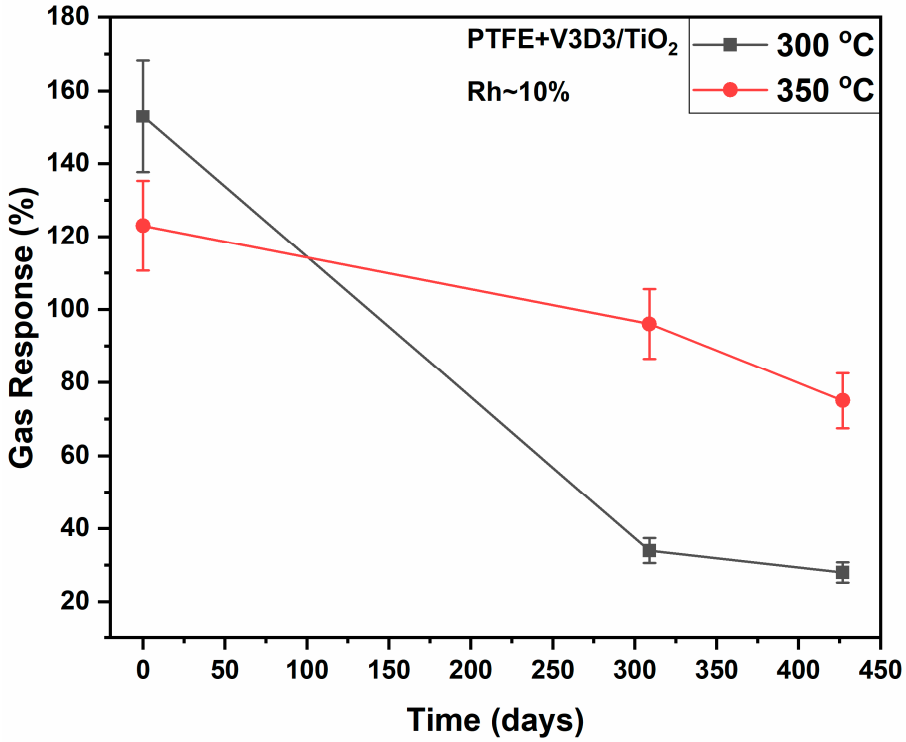


Figure 6. Gas response of the P(V_3D_3-co-TFE)/TiO_2 hybrid structure to hydrogen gas at 300 °C (gray symbols) and 350 °C (red symbols) and 10% RH measured over a time span of 427 days.

This behavior must be taken into account when integrating the sensor into devices for applications such as human breath testing. It creates opportunities for further research, particularly in the development of mathematical control logics. Apart from the hydrogen gas response values, the optimum operation temperature also experiences changes. The initial measurement (Figure 3) indicates an optimum operation temperature of 300 °C, while the second and third measurements show the highest response values and consequently better operation conditions at 350 °C. A similar trend can be observed for the determination of the LoD (Figure S3).

In this context, it should be noted that elevated temperatures for sensor operation could have an annealing effect on the presented hybrid sensors. As mentioned previously, PTFE usually cannot withstand operating temperatures higher than 320 °C, whereas PV_3D_3 usually retains its properties even at 400 °C. As indicated in Figure 2, the used copolymer does not show significant signs of decomposition, but rather slight changes of the internal ring structure. These structural changes occur during the first measurements at elevated temperatures, which could result in the observed shift of optimum operation temperature from 300 to 350 °C in all subsequent measurements. This phenomenon of enhanced performance at higher operation temperature can also be attributed to the underlying metal oxide sensing structure. However, conflicting observations have been made regarding the optimum temperature. While some studies suggest a peak performance around 300–350 °C [15,45], others indicate continuous performance enhancement with increasing temperature [20]. The parameters determined in this work, such as operating temperature

and response value, enable a comparison of the TiO_2 sensor with additional P(V_3D_3-co-TFE) coating with different polymer-containing sensors used in the gas sensing industry. As seen in Table 1, scientists have experimented with different hybrid structures for the detection of a variety of different gases. The number of publications in this area is relatively limited and focusses particularly on the use of conductive copolymers, while non-conductive polymers have yet to be further explored.

Table 1. Copolymer coatings studied in the gas sensor industry.

No.	Sensing Material	Polymer	Target	OPT, °C	Concentration	Response	Ref.
1.	ZIF-8/PDMS	PDMS	CH_4	-	50%	16%	[82]
2.	PANI-co-PIN /Cu–Al_2O_3	PANI-co-PIN	Ammonia	RT	-	8 μΩ *	[83]
3.	(PANA-*Co*-PIN): Fe_3O_4-	(PANA-*Co*-PIN)	Ammonia	-	-	7 μΩ *	[84]
4.	TiO_2-g-P(SPEA-co-GMA)	P(SPEA-co-GMA)	Light Responsiveness	-	-	-	[85]
5.	PANI-*co*-PPy/Cu-Al_2O_3	(PANI-*co*-PPy)	Ammonia	RT	100 ppm	5 μΩ *	[86]
6.	PLANC-GOD	PLANC	Glucose	-	1; 3; 5; 7; 10^{-6} mol L	-	[87]
7.	(EMAA)/(MWCNT)	EMAA	Strain sensing	220	-	41.1 S m^{-1}	[88]
D1	P(V3D3-co-TFE)/TiO_2	P(V3D3-co-TFE)	H_2	300	100 ppm	153%	T.w.
D1	P(V3D3-co-TFE)/TiO_2	P(V3D3-co-TFE)	H_2	350	100 ppm	123%	T.w.

*—estimated from graphs; T.w. = this work; D1 = dataset from Figure 1; PDMS = poly (dimethylsiloxane); PANI = polyaniline; PIN = polyindole; PANA = poly(anthranilic acid); SPEA = poly(spiropyran ethylacrylate); PGMA = poly(glycidyl methacrylate); PPy = polypyrrole; PLANC = poly(luminol–aniline) nanowires composite; PEMAA = poly(ethylene-co-methacrylic acid); PV_3D_3 = poly(trivinyltrimethylcyclotrisiloxane); PTFE = polytetrafluoroethylene.

Table 2 compares the hybrid sensors reported in this study with selected hydrogen detectors coated with conventional polymers. Notably, the reaction and recovery times achieved are relatively fast in comparison with sensors from the literature. In addition, despite the very low concentrations of 100 ppm used in our experiment, high hydrogen response values were obtained, exceeding even those of sensors tested in higher initial concentrations. The relative humidity varies for the measurement in most test setups.

Table 2. Polymer-coated H_2 detectors studied in sensor industry and publications.

No.	Sensing Material	Polymer	H2 Concentration	RH, ~%	OPT, °C	Response	Time, s		Ref.
							Response	Recovery	
1.	TiO_2	PV4D4	100 ppm	-	300	100%	3	44	[15]
2.	TiO_2	PV4D4	100 ppm	-	350	709.07%	3.02	23.23	[20]
3.	PEDOT:PSS@Pd	PEDOT: PSS	4 %	-	RT	31.6%	19 (±4)	73 (±11)	[89]
4.	PANI/SnO_2	PANI	6000 ppm	-	RT	42%	11	7	[90]
5.	PANI/Al-SnO_2	PANI	1000 ppm	-	48	-	2	2	[91]
6.	PANI/Al-SnO_2	PANI	100 ppm	-	340	-	3	2	[91]
7.	PANI/SnO_2 + Pd	PANI	50 ppm	-	RT	19.2%	39	53	[92]
8.	PANI/SnO_2 + Pd	PANI	350 ppm	-	RT	353.7%	141	76	[92]
9.	PMMA/SnO_2:In_2O_3	PMMA	600 ppm	14	RT	1.05×10^3 Ω	196	282	[93]
10.	PMMA/SnO_2:In_2O_3	PMMA	600 ppm	65	RT	1.34×10^2 Ω	842	387	[93]
11.	Cytop/SnO_2:In_2O_3	Cytop	600 ppm	14	RT	1.49×10^1 Ω	1550	35	[93]
12.	Cytop/SnO_2:In_2O_3	Cytop	600 ppm	65	RT	7.52×10^1 Ω	322	44	[93]
13.	Fluoropel/SnO_2:In_2O_3	fluoropolymer	600 ppm	14	RT	1.55×10^2 Ω	134	30	[93]
14.	Fluoropel/SnO_2:In_2O_3	fluoropolymer	600 ppm	65	RT	9.79×10^1 Ω	356	56	[93]

Table 2. *Cont.*

No.	Sensing Material	Polymer	H2 Concentration	RH, ~%	OPT, °C	Response	Time, s		Ref.
							Response	Recovery	
D2	P(V3D3-co-TFE)/TiO_2	P(V3D3-co-TFE)	100 ppm	10	300	34%	3	4.9	T.w.
D2	P(V3D3-co-TFE)/TiO_2	P(V3D3-co-TFE)	100 ppm	10	350	96%	1.3	2.1	T.w.
D2	P(V3D3-co-TFE)/TiO_2	P(V3D3-co-TFE)	100 ppm	45	300	23%	4.2	4.4	T.w.
D2	P(V3D3-co-TFE)/TiO_2	P(V3D3-co-TFE)	100 ppm	45	350	73%	2.3	3.3	T.w.
D3	P(V3D3-co-TFE)/TiO_2	P(V3D3-co-TFE)	100 ppm	10	300	28%	1.5	3.1	T.w.
D3	P(V3D3-co-TFE)/TiO_2	P(V3D3-co-TFE)	100 ppm	10	350	75%	2.5	3.2	T.w.
D3	P(V3D3-co-TFE)/TiO_2	P(V3D3-co-TFE)	100 ppm	45	300	23%	1.7	2.1	T.w.
D3	P(V3D3-co-TFE)/TiO_2	P(V3D3-co-TFE)	100 ppm	45	350	48%	1.7	3.5	T.w.

T.w. = this work; D2 = dataset from Figure 2; D3 = dataset from Figure S1; PV4D4 = poly(1,3,5,7-tetramethyl-tetravinylcyclotetrasiloxane); PEDOT = poly(3,4-ethylenedioxythiophene); PSS = poly(styrene sulfonate); PANI = polyaniline; PMMA = polymethyl methacrylate; Cytop = poly-perfluorobutenyl vinyl ether; PV3D3 = poly (trivinyltrimethyltrimethylcyclotrisiloxane); PTFE = polytetrafluoroethylene.

On the other hand, in Table 3 one can see our previous research on the materials used in this work, which have been adapted through various improvement processes.

Table 3. Comparison of all our previous works results with different sensing structures and coatings for gas detection.

Sensing Structure	Polymer Coating	Enhancement	OPT, °C	Detected Gas	Gas Response, %	Ref.
TiO_2	Uncoated	TA 450 °C	250	Hydrogen	600	[22]
TiO_2	PTFE	-	350	2-propanol	64	[46]
TiO_2	PV4D4	-	400	2-propanol	225	[45]
TiO_2	PV4D4	TA 610 °C for TiO_2	300/RT	Hydrogen/ Ammonia	100/52	[15]
TiO_2	PV4D4	TA 450 °C for PV4D4	350	Hydrogen	709	[20]
CuO/Cu_2O/ZnO:Fe	PV3D3	RTA 650 °C	350	Hydrogen	191	[39]
TiO_2	PV3D3	-	-	-	-	To be published
TiO_2	P(V3D3 + TFE)	Copolymer structure	300	Hydrogen	153	This work

TA—thermal annealing; RTA—rapid thermal annealing.

4. Conclusions

This study demonstrates that the proposed P(V_3D_3-co-TFE)/TiO_2 hybrid sensor is relatively reliable over an extended period of time. It exhibits hydrogen selectivity in different environments demanded for different application fields such as in cleanrooms, biomedical applications, or food storage. Tests at 10% RH are necessary to isolate the hydrogen response [94], because the sensor materials can adsorb water molecules which can influence the gas response. Even after a total of 427 days, similar trends were observed in all experimental measurements. An optimum operating temperature of 300 and 350 °C and a constant selectivity for hydrogen gas were determined. The elevated operating temperatures do not lead to a significant decomposition of the P(V_3D_3-co-TFE) film according to our experiments. A change in the internal structure was rather observed from FTIR studies. While the selectivity remains constant, the overall response values to hydrogen gas decrease slightly over time; namely, they were reduced to approximately 75% at 350 °C operating temperature. Nevertheless, it is possible to integrate this type of sensor structure with constant selectivity into smart devices where a response time curve is used to filter all the collected data. Hence, it can be applied not only as a simple detector,

but rather as a potential exhaled breath detector for diagnostics or a feedback system for industrial applications. This provides new pathways to tune the gas sensor performance for specific applications. The applied copolymer thin film can introduce novel, e.g., sieve-like structures that enhance selectivity, sensitivity, and stability for preexisting sensor structures. Future research could investigate the potential tailoring of the additional polymer films to enhance the functionality in the context of molecular polymer–gas interactions. Different co-monomer combinations could give rise to sensors which are specifically tailored for certain gases and applications. Nevertheless, more research could be performed on this type of hybrid sensors, taking into consideration even other aspects, from an electronic device point of view, such as performing experiments at different magnetic fields [42], finding factors on how to improve self-healing and improve relationships between polymer breakdown strength and permittivity [40], adding ferromagnetic components [43], and further stoichiometry as in similar research [44]. In this regard, this research will and must continue to obtain reliable results and improve both the medical and industrial fields.

Supplementary Materials: The following supporting information can be downloaded at: https://www.mdpi.com/article/10.3390/chemosensors13040150/s1, Figure S1. The gas response of the TiO_2 structure, coated with a thin layer of V3D3 copolymer and PTFE, namely P(V3D3-co-TFE)/TiO_2 hybrid structures, after 427 days from 1st measurements, to different gases and VOCs (hydrogen, methane, carbon dioxide, ethanol, acetone, acetone, 2-propanol, n-butanol, ammonia) at different operating temperatures for relative humidity of (a) ~10% RH and (b) ~45% RH; Figure S2. Dynamic response of TiO_2 sensing structure coated with a thin layer of V3D3 copolymer and PTFE, namely P(V3D3-co-TFE)/TiO_2 hybrid structures, after 427 days from 1st measurements, to hydrogen vapor at different operating temperatures and different relative humidity: (a) 300 °C, ~10% RH; (b) 300 °C, ~45% RH; (c) 350 °C, ~10% RH and (d) 350 °C, ~45% RH; Figure S3. Limit-of-detection graph for H_2-sensing hybrid sensor, namely P(V3D3-co-TFE)/TiO_2 hybrid structures, at different concentrations, for different relative humidity and operating temperatures: (1) 300 °C, ~10% RH; (2) 300 °C, ~45% RH; (3) 350 °C, ~10% RH and (4) 350 °C, ~45% RH.

Author Contributions: Conceptualization, O.L., F.F., and S.S.; methodology, O.L., M.B., R.A., and S.S.; software, S.S., T.A., M.B., and L.S.; validation, F.F., R.A., O.L., S.S., T.A., T.S., L.Z., T.P., and B.V.; formal analysis, M.B., B.V., and L.S.; investigation, M.B., L.S., B.V., L.Z., O.L., and T.P.; resources, F.F., R.A., T.P., and B.V.; data curation, O.L., T.A., and T.S.; writing—original draft preparation, M.B., S.S., L.S., and O.L.; writing—review and editing, O.L, R.A., T.P., B.V., T.A., T.S., and L.Z.; visualization, L.S., M.B., and S.S.; supervision T.S., O.L., F.F., and T.A.; project administration, O.L. and F.F.; funding acquisition, F.F., R.A., and T.P. All authors have read and agreed to the published version of the manuscript.

Funding: We would also like to acknowledge the Government of the Republic of Moldova, Ministry of Education and Science for partial support via the State Program LIFETECH No. 020404 at the Technical University of Moldova. Mihai Brinza gratefully acknowledges Kiel University, Department of Materials Science, Chair for Multicomponent Materials, Chair of Functional Nanomaterials, Germany for internship positions in 2024-2025 and TUM for constant support. In addition, this work was partially funded by the German Research Foundation (DFG)—Project-ID 541212717 and Project-ID 286471992-SFB1261 project A2.

Institutional Review Board Statement: Not applicable.

Informed Consent Statement: Not applicable.

Data Availability Statement: The original contributions presented in this study are included in the article. Further inquiries can be directed to the corresponding authors.

Acknowledgments: O.L. gratefully acknowledges CNRS Council for support as an expert scientist at IRCP Chimie ParisTech, Paris, France. Mihai Brinza gratefully acknowledges Kiel University, Department of Materials Science, Chair for Multicomponent Materials, Chair of Functional Nanomaterials,

Germany for internship positions in 2024–2025 and TUM for constant support. We would also like to acknowledge the Government of the Republic of Moldova for partial support via the State Program LIFETECH No. 020404 at the Technical University of Moldova.

Conflicts of Interest: The authors declare no conflicts of interest.

References

1. Meixner, H.; Lampe, U. Metal Oxide Sensors. *Sens. Actuators B Chem.* **1996**, *33*, 198–202. [CrossRef]
2. Lenz, J.; Edelstein, S. Magnetic Sensors and Their Applications. *IEEE Sens. J.* **2006**, *6*, 631–649. [CrossRef]
3. Loock, H.-P.; Wentzell, P.D. Detection Limits of Chemical Sensors: Applications and Misapplications. *Sens. Actuators B Chem.* **2012**, *173*, 157–163. [CrossRef]
4. Arcos, J.M.M.; Santos, D.M.F. The Hydrogen Color Spectrum: Techno-Economic Analysis of the Available Technologies for Hydrogen Production. *Gases* **2023**, *3*, 25–46. [CrossRef]
5. Okolie, J.A.; Patra, B.R.; Mukherjee, A.; Nanda, S.; Dalai, A.K.; Kozinski, J.A. Futuristic Applications of Hydrogen in Energy, Biorefining, Aerospace, Pharmaceuticals and Metallurgy. *Int. J. Hydrogen Energy* **2021**, *46*, 8885–8905. [CrossRef]
6. Falcone, P.M.; Hiete, M.; Sapio, A. Hydrogen Economy and Sustainable Development Goals: Review and Policy Insights. *Curr. Opin. Green Sustain. Chem.* **2021**, *31*, 100506. [CrossRef]
7. Barthelemy, H.; Weber, M.; Barbier, F. Hydrogen Storage: Recent Improvements and Industrial Perspectives. *Int. J. Hydrogen Energy* **2017**, *42*, 7254–7262. [CrossRef]
8. Murugesan, K.; Senthamarai, T.; Chandrashekhar, V.G.; Natte, K.; Kamer, P.C.J.; Beller, M.; Jagadeesh, R.V. Catalytic Reductive Aminations Using Molecular Hydrogen for Synthesis of Different Kinds of Amines. *Chem. Soc. Rev.* **2020**, *49*, 6273–6328. [CrossRef]
9. Ciriminna, R.; Albanese, L.; Meneguzzo, F.; Pagliaro, M. Hydrogen Peroxide: A Key Chemical for Today's Sustainable Development. *ChemSusChem* **2016**, *9*, 3374–3381. [CrossRef]
10. Iida, A.; Nosaka, N.; Yumoto, T.; Knaup, E.; Naito, H.; Nishiyama, C.; Yamakawa, Y.; Tsukahara, K.; Terado, M.; Sato, K.; et al. The Clinical Application of Hydrogen as a Medical Treatment. *Acta Med. Okayama* **2016**, *70*, 331–337. [CrossRef]
11. Zhang, J.-Y.; Liu, C.; Zhou, L.; Qu, K.; Wang, R.; Tai, M.; Lei Lei, J.W.; Wu, Q.F.; Wang, Z. A Review of Hydrogen as a New Medical Therapy. *Hepatogastroenterology* **2012**, *59*, 1026. [CrossRef] [PubMed]
12. Ostojic, S. Molecular Hydrogen in Sports Medicine: New Therapeutic Perspectives. *Int. J. Sports Med.* **2014**, *36*, 273–279. [CrossRef] [PubMed]
13. Huang, C.-S.; Kawamura, T.; Toyoda, Y.; Nakao, A. Recent Advances in Hydrogen Research as a Therapeutic Medical Gas. *Free Radic. Res.* **2010**, *44*, 971–982. [CrossRef] [PubMed]
14. Ohta, S. Recent Progress Toward Hydrogen Medicine: Potential of Molecular Hydrogen for Preventive and Therapeutic Applications. *Curr. Pharm. Des.* **2011**, *17*, 2241–2252. [CrossRef]
15. Brinza, M.; Schröder, S.; Ababii, N.; Gronenberg, M.; Strunskus, T.; Pauporté, T.; Adelung, R.; Faupel, F.; Lupan, O. Two-in-One Sensor Based on PV4D4-Coated TiO_2 Films for Food Spoilage Detection and as a Breath Marker for Several Diseases. *Biosensors* **2023**, *13*, 538. [CrossRef]
16. Ghawanmeh, A.A.; A.Tanash, S.; Al-Rawashdeh, N.A.F.; Albiss, B. The Recent Progress on Nanomaterial-Based Chemosensors for Diagnosis of Human Exhaled Breath: A Review. *J. Mater. Sci.* **2024**, *59*, 8573–8605. [CrossRef]
17. Kerlin, P.; Wong, L. Breath Hydrogen Testing in Bacterial Overgrowth of the Small Intestine. *Gastroenterology* **1988**, *95*, 982–988. [CrossRef] [PubMed]
18. De Geyter, C.; Van de Maele, K.; Hauser, B.; Vandenplas, Y. Hydrogen and Methane Breath Test in the Diagnosis of Lactose Intolerance. *Nutrients* **2021**, *13*, 3261. [CrossRef]
19. Marton, A.; Xue, X.; Szilagyi, A. Meta-analysis: The Diagnostic Accuracy of Lactose Breath Hydrogen or Lactose Tolerance Tests for Predicting the North European Lactase Polymorphism C/T-13910. *Aliment. Pharmacol. Ther.* **2012**, *35*, 429–440. [CrossRef]
20. Lupan, O.; Brinza, M.; Piehl, J.; Ababii, N.; Magariu, N.; Zimoch, L.; Strunskus, T.; Pauporté, T.; Adelung, R.; Faupel, F.; et al. Influence of Silsesquioxane-Containing Ultra-Thin Polymer Films on Metal Oxide Gas Sensor Performance for the Tunable Detection of Biomarkers. *Chemosensors* **2024**, *12*, 76. [CrossRef]
21. Lupan, O.; Brinza, M.; Schroder, S.; Ababii, N.; Strunskus, T.; Viana, B.; Pauporté, T.; Adelung, R.; Faupel, F. Sensors Based on Hybrid Materials for Environmental, Industrial and Biomedical Applications. In Proceedings of the 2024 IEEE 14th International Conference "Nanomaterials: Applications and Properties" (NAP 2024), Riga, Latvia, 8–13 September 2024; Institute of Electrical and Electronics Engineers Inc.: Piscataway, NJ, USA, 2024. [CrossRef]
22. Lupan, O.; Postica, V.; Ababii, N.; Reimer, T.; Shree, S.; Hoppe, M.; Polonskyi, O.; Sontea, V.; Chemnitz, S.; Faupel, F.; et al. Ultra-Thin TiO_2 Films by Atomic Layer Deposition and Surface Functionalization with Au Nanodots for Sensing Applications. *Mater. Sci. Semicond. Process.* **2018**, *87*, 44–53. [CrossRef]

23. Fan, G.; Guan, J.; Yu, H.; Zhu, Q.; Han, N.; Mo, J.; Chen, Y. Highly Sensitive Formaldehyde Gas Sensor Based on SnO_2/Zn_2SnO_4 Hybrid Structures. *Build. Environ.* **2024**, *262*, 111781. [CrossRef]
24. Sakalley, S.; Saravanan, A.; Kathiravan, D.; Tang, J.-C.; Cheng, W.-C.; Chen, S.-C.; Sun, H.; Huang, B.-R. Enhanced Hydrogen Gas Sensing through the Utilization of a Hybrid Nanostructure Combining ZnO Nanotubes and HiPIMS Cu3N Thin Film. *Sens. Actuators B Chem.* **2024**, *402*, 135107. [CrossRef]
25. Nirmala Devi, K.; Vadivel, S. Room Temperature Fiber Optic Gas Sensor Technology Based Zn3(VO4)2/PMMA Hybrid Composites via Facile Hydrothermal Route. *Opt. Fiber Technol.* **2024**, *82*, 103642. [CrossRef]
26. Lupan, O.; Santos-Carballal, D.; Ababii, N.; Magariu, N.; Hansen, S.; Vahl, A.; Zimoch, L.; Hoppe, M.; Pauporté, T.; Galstyan, V.; et al. $TiO_2/Cu_2O/CuO$ Multi-Nanolayers as Sensors for H_2 and Volatile Organic Compounds: An Experimental and Theoretical Investigation. *ACS Appl. Mater. Interfaces* **2021**, *13*, 32363–32380. [CrossRef]
27. Sari, Y.; Gareso, P.L.; Armynah, B.; Tahir, D. A Review of TiO_2 Photocatalyst for Organic Degradation and Sustainable Hydrogen Energy Production. *Int. J. Hydrogen Energy* **2024**, *55*, 984–996. [CrossRef]
28. Seremak, W.; Jasiorski, M.; Baszczuk, A.; Winnicki, M. Durability Assessment of Low-Pressure Cold-Sprayed TiO_2 Photocatalytic Coatings: Photocatalytic and Mechanical Stability. *Surf. Coat. Technol.* **2025**, *497*, 131740. [CrossRef]
29. Li, M.; Zhao, N.; Wang, C.; Zou, Y.; Chen, X.; Mei, Y. Improving Thermal Stability and Electrochemical Performance of Polymer Solid Electrolyte Membranes with a Novel TiO_2@PA-APP Composite Additive. *Colloids Surf. A Physicochem. Eng. Asp.* **2025**, *705*, 135640. [CrossRef]
30. Ferroni, M.; Guidi, V.; Martinelli, G.; Faglia, G.; Nelli, P.; Sberveglieri, G. Characterization of a Nanosized TiO2 Gas Sensor. *Nanostruct. Mater.* **1996**, *7*, 709–718. [CrossRef]
31. Li, Z.; Yao, Z.; Haidry, A.A.; Plecenik, T.; Xie, L.; Sun, L.; Fatima, Q. Resistive-Type Hydrogen Gas Sensor Based on TiO2: A Review. *Int. J. Hydrogen Energy* **2018**, *43*, 21114–21132. [CrossRef]
32. Malallah Rzaij, J.; Mohsen Abass, A. Review on: TiO_2 Thin Film as a Metal Oxide Gas Sensor. *J. Chem. Rev.* **2020**, *2*, 114–121. [CrossRef]
33. Lupan, O.; Ababii, N.; Mishra, A.K.; Bodduluri, M.T.; Magariu, N.; Vahl, A.; Krüger, H.; Wagner, B.; Faupel, F.; Adelung, R.; et al. Heterostructure-Based Devices with Enhanced Humidity Stability for H_2 Gas Sensing Applications in Breath Tests and Portable Batteries. *Sens. Actuators A Phys.* **2021**, *329*, 112804. [CrossRef]
34. Wang, C.; Yin, L.; Zhang, L.; Xiang, D.; Gao, R. Metal Oxide Gas Sensors: Sensitivity and Influencing Factors. *Sensors* **2010**, *10*, 2088–2106. [CrossRef]
35. Wicker, S.; Guiltat, M.; Weimar, U.; Hémeryck, A.; Barsan, N. Ambient Humidity Influence on CO Detection with SnO_2 Gas Sensing Materials. A Combined DRIFTS/DFT Investigation. *J. Phys. Chem. C* **2017**, *121*, 25064–25073. [CrossRef]
36. Enachi, M.; Lupan, O.; Braniste, T.; Sarua, A.; Chow, L.; Mishra, Y.K.; Gedamu, D.; Adelung, R.; Tiginyanu, I. Integration of Individual TiO_2 Nanotube on the Chip: Nanodevice for Hydrogen Sensing. *Phys. Status Solidi-Rapid Res. Lett.* **2015**, *9*, 171–174. [CrossRef]
37. Mahdavi, H.; Rahbarpour, S.; Hosseini-Golgoo, S.-M.; Jamaati, H. Reducing the Destructive Effect of Ambient Humidity Variations on Gas Detection Capability of a Temperature Modulated Gas Sensor by Calcium Chloride. *Sens. Actuators B Chem.* **2021**, *331*, 129091. [CrossRef]
38. Yamazoe, N.; Shimanoe, K. Fundamentals of Semiconductor Gas Sensors. In *Semiconductor Gas Sensors*; Elsevier: Amsterdam, The Netherlands, 2020; pp. 3–38. [CrossRef]
39. Schröder, S.; Ababii, N.; Lupan, O.; Drewes, J.; Magariu, N.; Krüger, H.; Strunskus, T.; Adelung, R.; Hansen, S.; Faupel, F. Sensing Performance of $CuO/Cu_2O/ZnO$:Fe Heterostructure Coated with Thermally Stable Ultrathin Hydrophobic PV3D3 Polymer Layer for Battery Application. *Mater. Today Chem.* **2022**, *23*, 100642. [CrossRef]
40. Guo, Y.; Zhou, D.; Li, D.; Zhao, W.; Wang, Y.; Pang, L.; Shi, Z.; Zhou, T.; Sun, S.; Singh, C.; et al. Improved Energy Storage Performance of Sandwich-Structured P(VDF-HFP)-Based Nanocomposites by the Addition of Inorganic Nanoparticles. *J. Mater. Chem. C* **2023**, *11*, 6999–7009. [CrossRef]
41. Lupan, C.; Kohlmann, N.; Petersen, D.; Bodduluri, M.T.; Buzdugan, A.; Jetter, J.; Quandt, E.; Kienle, L.; Adelung, R.; Lupan, O. Hydrogen Nanosensors Based on Core/Shell ZnO/Al_2O_3 and $ZnO/ZnAl_2O_4$ Single Nanowires. *Mater. Today Nano* **2025**, *29*, 100596. [CrossRef]
42. Trukhanov, A.V.; Turchenko, V.O.; Bobrikov, I.A.; Trukhanov, S.V.; Kazakevich, I.S.; Balagurov, A.M. Crystal Structure and Magnetic Properties of the $BaFe_{12-X}Al_XO_{19}$ (X=0.1–1.2) Solid Solutions. *J. Magn. Magn. Mater.* **2015**, *393*, 253–259. [CrossRef]
43. Trukhanov, S.V.; Troyanchuk, I.O.; Pushkarev, N.V.; Szymczak, H. Magnetic Properties of Anion-Deficient $La_{1-x}Ba_xMnO_{3-x/2}$ ($0 \leq x \leq 0.30$) Manganites. *J. Exp. Theor. Phys.* **2003**, *96*, 110–117. [CrossRef]
44. Trukhanov, S.V.; Trukhanov, A.V.; Stepin, S.G.; Szymczak, H.; Botez, C.E. Effect of the Size Factor on the Magnetic Properties of Manganite $La_{0.50}Ba_{0.50}MnO_3$. *Phys. Solid State* **2008**, *50*, 886–893. [CrossRef]

45. Schröder, S.; Ababii, N.; Brînză, M.; Magariu, N.; Zimoch, L.; Bodduluri, M.T.; Strunskus, T.; Adelung, R.; Faupel, F.; Lupan, O. Tuning the Selectivity of Metal Oxide Gas Sensors with Vapor Phase Deposited Ultrathin Polymer Thin Films. *Polymers* **2023**, *15*, 524. [CrossRef] [PubMed]
46. Schröder, S.; Brinza, M.; Cretu, V.; Zimoch, L.; Gronenberg, M.; Ababii, N.; Railean, S.; Strunskus, T.; Pauporté, T.; Adelung, R.; et al. *A New Approach in Detection of Biomarker 2-Propanol with PTFE-Coated TiO2 Nanostructured Films. Sontea, V., Tiginyanu, I., Railean, S., Eds.*; Springer Nature: Cham, Switzerland, 2024; pp. 75–83. ISBN 978-3-031-42782-4. [CrossRef]
47. Baker, B.B.; Kasprzak, D.J. Thermal Degradation of Commercial Fluoropolymers in Air. *Polym. Degrad. Stab.* **1993**, *42*, 181–188. [CrossRef]
48. Conesa, J.A.; Font, R. Polytetrafluoroethylene Decomposition in Air and Nitrogen. *Polym. Eng. Sci.* **2001**, *41*, 2137–2147. [CrossRef]
49. Hirai, D.; Sawai, O.; Nunoura, T.; Hiroi, Z. Facile Synthetic Route to Transition Metal Oxyfluorides via Reactions between Metal Oxides and PTFE. *J. Fluor. Chem.* **2018**, *209*, 43–48. [CrossRef]
50. Tenhaeff, W.E.; Gleason, K.K. Initiated and Oxidative Chemical Vapor Deposition of Polymeric Thin Films: ICVD and OCVD. *Adv. Funct. Mater.* **2008**, *18*, 979–992. [CrossRef]
51. Wang, P.; Shao, Z.; Ulfa, M.; Pauporté, T. Insights into the Hole Blocking Layer Effect on the Perovskite Solar Cell Performance and Impedance Response. *J. Phys. Chem. C* **2017**, *121*, 9131–9141. [CrossRef]
52. Lupan, O.; Ababii, N.; Santos-Carballal, D.; Terasa, M.-I.M.-I.; Magariu, N.; Zappa, D.; Comini, E.; Pauporté, T.; Siebert, L.; Faupel, F.; et al. Tailoring the Selectivity of Ultralow-Power Heterojunction Gas Sensors by Noble Metal Nanoparticle Functionalization. *Nano Energy* **2021**, *88*, 106241. [CrossRef]
53. Hoppe, M.; Ababii, N.; Postica, V.; Lupan, O.; Polonskyi, O.; Schütt, F.; Kaps, S.; Sukhodub, L.F.; Sontea, V.; Strunskus, T.; et al. (CuO-Cu_2O)/ZnO:Al Heterojunctions for Volatile Organic Compound Detection. *Sens. Actuators B Chem.* **2018**, *255*, 1362–1375. [CrossRef]
54. Schröder, S.; Polonskyi, O.; Strunskus, T.; Faupel, F. Nanoscale Gradient Copolymer Films via Single-Step Deposition from the Vapor Phase. *Mater. Today* **2020**, *37*, 35–42. [CrossRef]
55. Rappe, A.K.; Casewit, C.J.; Colwell, K.S.; Goddard, W.A.; Skiff, W.M. UFF, a Full Periodic Table Force Field for Molecular Mechanics and Molecular Dynamics Simulations. *J. Am. Chem. Soc.* **1992**, *114*, 10024–10035. [CrossRef]
56. Lupan, O.; Postica, V.; Pauporté, T.; Viana, B.; Terasa, M.-I.; Adelung, R. Room Temperature Gas Nanosensors Based on Individual and Multiple Networked Au-Modified ZnO Nanowires. *Sens. Actuators B Chem.* **2019**, *299*, 126977. [CrossRef]
57. Park, S.Y.; Kim, Y.H.; Lee, S.Y.; Sohn, W.; Lee, J.-H.J.E.; Kim, D.H.; Shim, Y.-S.; Kwon, K.C.; Choi, K.S.; Yoo, H.J.; et al. Highly Selective and Sensitive Chemoresistive Humidity Sensors Based on RGO/MoS 2 van Der Waals Composites. *J. Mater. Chem. A* **2018**, *6*, 5016–5024. [CrossRef]
58. Lupan, O.; Ababii, N.; Mishra, A.K.; Gronenberg, O.; Vahl, A.; Schürmann, U.; Duppel, V.; Krüger, H.; Chow, L.; Kienle, L.; et al. Single CuO/Cu_2O/Cu Microwire Covered by a Nanowire Network as a Gas Sensor for the Detection of Battery Hazards. *ACS Appl. Mater. Interfaces* **2020**, *12*, 42248–42263. [CrossRef]
59. Postica, V. Proprietăţile Senzoriale Ale Structurilor Hibride În Bază de Oxizi Metalici Şi a Reţelelor Lor. Ph.D. Thesis, Technical Univeristy of Moldova, Chișinău, Moldova, 2020.
60. Ding, K.; Zhang, D.; Jiang, L.; Chen, J.; Qu, R.; Shi, F.; Li, B.; He, X.; Wang, L.; Wang, H. An Ionic Liquid-Present Immersion Method for Preparing Cotton Fiber-Shaped Cu_2O Nanoparticles at Room Temperature. *J. Appl. Electrochem.* **2022**, *52*, 55–65. [CrossRef]
61. Nakate, U.; Yu, Y.-T.; Park, S. Hierarchical CuO Nanostructured Materials for Acetaldehyde Sensor Application. *Microelectron. Eng.* **2022**, *251*, 111662. [CrossRef]
62. Chen, Z.; Jiang, Z.-Y.; Deng, S.; Hou, M.; Zhang, X.; Jiang, Z.; Lai, N.-C. Morphology-Controlled Synthesis of Cu_2O Encapsulated Phase Change Materials: Photothermal Conversion and Storage Performance in Visible Light Regime. *Chem. Eng. J.* **2023**, *454*, 140089. [CrossRef]
63. Helwig, N.; Schüler, M.; Bur, C.; Schütze, A.; Sauerwald, T. Gas Mixing Apparatus for Automated Gas Sensor Characterization. *Meas. Sci. Technol.* **2014**, *25*, 055903. [CrossRef]
64. Luo, S.; Shen, Y.; Wu, Z.; Cao, M.; Gu, F.; Wang, L. Enhanced Ethanol Sensing Performance of Mesoporous Sn-Doped ZnO. *Mater. Sci. Semicond. Process.* **2016**, *41*, 535–543. [CrossRef]
65. Brunetti, B.; Desimoni, E. About Estimating the Limit of Detection by the Signal to Noise Approach. *Pharm. Anal. Acta* **2015**, *06*, 1–4. [CrossRef]
66. Cretu, V.; Postica, V.; Mishra, A.K.; Hoppe, M.; Tiginyanu, I.; Mishra, Y.K.; Chow, L.; de Leeuw, N.H.; Adelung, R.; Lupan, O. Synthesis, Characterization and DFT Studies of Zinc-Doped Copper Oxide Nanocrystals for Gas Sensing Applications. *J. Mater. Chem. A* **2016**, *4*, 6527–6539. [CrossRef]
67. Biadasz, A.; Kotkowiak, M.; Łukawski, D.; Jadwiżak, J.; Rytel, K.; Kędzierski, K. A Versatile Gas Transmission Device with Precise Humidity Control for QCM Humidity Sensor Characterizations. *Measurement* **2022**, *200*, 111674. [CrossRef]

68. O'Shaughnessy, W.S.; Gao, M.; Gleason, K.K. Initiated Chemical Vapor Deposition of Trivinyltrimethylcyclotrisiloxane for Biomaterial Coatings. *Langmuir* **2006**, *22*, 7021–7026. [CrossRef]
69. Piwowarczyk, J.; Jędrzejewski, R.; Moszyński, D.; Kwiatkowski, K.; Niemczyk, A.; Baranowska, J. XPS and FTIR Studies of Polytetrafluoroethylene Thin Films Obtained by Physical Methods. *Polymers* **2019**, *11*, 1629. [CrossRef]
70. Du, W.; Tu, J.; Qiu, M.; Zhou, S.; Luo, Y.; Ong, W.-L.; Zhao, J. Temperature-Mediated Structural Evolution of Vapor–Phase Deposited Cyclosiloxane Polymer Thin Films for Enhanced Mechanical Properties and Thermal Conductivity. *Int. J. Extrem. Manuf.* **2023**, *5*, 025101. [CrossRef]
71. Ziegler, V.; Paraginski, R.T.; Ferreira, C.D. Grain Storage Systems and Effects of Moisture, Temperature and Time on Grain Quality—A Review. *J. Stored Prod. Res.* **2021**, *91*, 101770. [CrossRef]
72. Esrafili, A.; Wagner, A.; Inamdar, S.; Acharya, A.P. Covalent Organic Frameworks for Biomedical Applications. *Adv. Healthc. Mater.* **2021**, *10*, 2002090. [CrossRef]
73. Wolkoff, P.; Azuma, K.; Carrer, P. Health, Work Performance, and Risk of Infection in Office-like Environments: The Role of Indoor Temperature, Air Humidity, and Ventilation. *Int. J. Hyg. Environ. Health* **2021**, *233*, 113709. [CrossRef]
74. Ma, Z.; Fei, T.; Zhang, T. An Overview: Sensors for Low Humidity Detection. *Sens. Actuators B Chem.* **2023**, *376*, 133039. [CrossRef]
75. Sofia Paulino Mendes, A.; Rutgersson, A.; Paulsson, M. Outdoor Environmental Effects on Cleanrooms—A Study from a Swedish Hospital Pharmacy Compounding Unit. *Eur. J. Pharm. Biopharm.* **2022**, *177*, 100–106. [CrossRef] [PubMed]
76. Sikka, M.P.; Mondal, M. A Critical Review on Cleanroom Filtration. *Res. J. Text. Appar.* **2022**, *26*, 452–467. [CrossRef]
77. Meng, H.; Shiue, A.; Wang, C.; Liu, J.; Jia, L.; Leggett, G. Particle and Bacterial Colony Emissions from Garments and Humans in Pharmaceutical Cleanrooms. *J. Build. Eng.* **2024**, *97*, 110829. [CrossRef]
78. Lobanchykova, N.M.; Vakaliuk, T.A.; Korbut, V.P.; Lobanchykov, S.M.; Krasnov, Y.B. Features of Designing Systems for the Formation of an Internal Microclimate of a High Class of Cleanliness of Operating Rooms of Medical Institutions. *IOP Conf. Ser. Earth Environ. Sci.* **2024**, *1415*, 012124. [CrossRef]
79. Dey, A. Semiconductor Metal Oxide Gas Sensors: A Review. *Mater. Sci. Eng. B* **2018**, *229*, 206–217. [CrossRef]
80. Shin, W.; Hong, S.; Jeong, Y.; Jung, G.; Park, J.; Kim, D.; Choi, K.; Shin, H.; Koo, R.-H.; Kim, J.-J.; et al. Low-Frequency Noise in Gas Sensors: A Review. *Sens. Actuators B Chem.* **2023**, *383*, 133551. [CrossRef]
81. Chaoumead, A.; Joo, B.-H.; Kwak, D.-J.; Sung, Y.-M. Structural and Electrical Properties of Sputtering Power and Gas Pressure on Ti-Dope In2O3 Transparent Conductive Films by RF Magnetron Sputtering. *Appl. Surf. Sci.* **2013**, *275*, 227–232. [CrossRef]
82. Cao, R.; Ding, H.; Kim, K.-J.; Peng, Z.; Wu, J.; Culp, J.T.; Ohodnicki, P.R.; Beckman, E.; Chen, K.P. Metal-Organic Framework Functionalized Polymer Coating for Fiber Optical Methane Sensors. *Sens. Actuators B Chem.* **2020**, *324*, 128627. [CrossRef]
83. Sankar, S.; George, A.; Ramesan, M.T. Copper Alumina @ Poly (Aniline- Co -Indole) Nanocomposites: Synthesis, Characterization, Electrical Properties and Gas Sensing Applications. *RSC Adv.* **2022**, *12*, 17637–17644. [CrossRef] [PubMed]
84. Jayakrishnan, P.; Jithin, K.; Meera, K.; Ramesan, M.T. Synthesis, Characterization, Magnetoelectric Properties and Gas Sensing Application of Poly(Anthranilic Acid- Co- Indole)/ Magnetite Nanocomposites. *J. Thermoplast. Compos. Mater.* **2023**, *36*, 2523–2542. [CrossRef]
85. Arjmand, F.; Mohamadnia, Z. Fabrication of a Light-Responsive Polymer Nanocomposite Containing Spiropyran as a Sensor for Reversible Recognition of Metal Ions. *Polym. Chem.* **2022**, *13*, 937–945. [CrossRef]
86. Sankar, S.; Ramesan, M.T. Synthesis, Characterization, Conductivity, and Gas-sensing Performance of Copolymer Nanocomposites Based on Copper Alumina and Poly(Aniline-Co-pyrrole). *Polym. Eng. Sci.* **2022**, *62*, 2402–2410. [CrossRef]
87. Li, G.; Lian, J.; Zheng, X.; Cao, J. Electrogenerated Chemiluminescence Biosensor for Glucose Based on Poly(Luminol–Aniline) Nanowires Composite Modified Electrode. *Biosens. Bioelectron.* **2010**, *26*, 643–648. [CrossRef] [PubMed]
88. Hia, I.L.; Snyder, A.D.; Turicek, J.S.; Blanc, F.; Patrick, J.F.; Therriault, D. Electrically Conductive and 3D-Printable Copolymer/MWCNT Nanocomposites for Strain Sensing. *Compos. Sci. Technol.* **2023**, *232*, 109850. [CrossRef]
89. Zhu, Z.; Liu, C.; Jiang, F.; Liu, J.; Liu, G.; Ma, X.; Liu, P.; Huang, R.; Xu, J.; Wang, L. Flexible Fiber-Shaped Hydrogen Gas Sensor via Coupling Palladium with Conductive Polymer Gel Fiber. *J. Hazard. Mater.* **2021**, *411*, 125008. [CrossRef] [PubMed]
90. Sonwane, N.D.; Maity, M.D.; Kondawar, S.B. Conducting Polyaniline/SnO2 Nanocomposite for Room Temperature Hydrogen Gas Sensing. *Mater. Today Proc.* **2019**, *15*, 447–453. [CrossRef]
91. Sharma, H.J.; Jamkar, D.V.; Kondawar, S.B. Electrospun Nanofibers of Conducting Polyaniline/Al-SnO_2 Composites for Hydrogen Sensing Applications. *Procedia Mater. Sci.* **2015**, *10*, 186–194. [CrossRef]
92. Pippara, R.K.; Chauhan, P.S.; Yadav, A.; Kishnani, V.; Gupta, A. Room Temperature Hydrogen Sensing with Polyaniline/SnO_2/Pd Nanocomposites. *Micro Nano Eng.* **2021**, *12*, 100086. [CrossRef]

93. Kumar, A.; Zhang, P.; Vincent, A.; McCormack, R.; Kalyanaraman, R.; Cho, H.J.; Seal, S. Hydrogen Selective Gas Sensor in Humid Environment Based on Polymer Coated Nanostructured-Doped Tin Oxide. *Sens. Actuators B Chem.* **2011**, *155*, 884–892. [CrossRef]
94. Liu, Y.; Tian, Y.; Liu, F.; Gu, T.; Wang, B.; He, J.; Wang, C.; Meng, X.; Sun, P.; Lu, G. Multilayer Fluorine-Free MoBT x MBene with Hydrophilic Structural-Modulating for the Fabrication of a Low-Resistance and High-Resolution Humidity Sensor. *Adv. Sci.* **2024**, *11*, 2404178. [CrossRef]

Disclaimer/Publisher's Note: The statements, opinions and data contained in all publications are solely those of the individual author(s) and contributor(s) and not of MDPI and/or the editor(s). MDPI and/or the editor(s) disclaim responsibility for any injury to people or property resulting from any ideas, methods, instructions or products referred to in the content.